Development of tsunami model integrating several different grid systems

Yoshinori Shigihara and Koji Fujima
National Defense Academy, Japan

SUMMARY:
Fine resolution of digital topographic/bathymetric data-sets are available in coastal region of Japan, under a Cartesian coordinate system. These data-sets are applied to numerical simulation of near-field tsunami. On the other hand, numerical simulation of far-field tsunami is conducted based on spherical coordinate system. Nesting two domains with different resolutions and/or coordinate systems brings some inconveniences when modelling tsunami. This study aims to develop a tsunami numerical model which is capable to include several grid systems and facilitate the process of assembling domains of different resolutions. The assembly of structured domains (inner and outer) is achieved by constructing an intermediate unstructured grid or connector-domain between them. A numerical simulation consisting of a tsunami Gaussian-hump shape is used for validation by determining the energy transferred/retained in the inner domain. In addition a practical application, the 2010 Chilean Tsunami, is provided as a case study to confirm the validity of proposed model.

Keywords: connector-domain, finite difference method, finite volume method, 2010 Chilean Tsunami

1. INTRODUCTION

Usually tsunami waves are modelled as long wave approximation within a Cartesian coordinate or a spherical coordinate system for their propagation. Nonlinear shallow water models based on the finite difference method can describe all tsunami physical processes from generation in deep oceans to coastal run-up. Since the wave celerity of tsunami depends on the water depth, i.e., $c=(gh)^{0.5}$, the tsunami wavelength becomes shorter in the shallower depth region. Thus, numerical simulation of tsunami is generally conducted through a series of nested grids, reducing the grid size as the wave gets shorter and thus maintaining an acceptable resolution of the waves in the shallower depth region.

Several grid-nesting schemes for tsunami modelling have been proposed, e.g., Kowalik and Murty (1993), Goto et al. (1997), Yamazaki et al. (2010) and Son et al. (2011). Most of these models adopt a two-way grid-nesting method, which is a system of two or more domains with different cell resolutions separated by a narrow domain boundary for the transition of rectangular cell between the two domain resolutions. The surface elevation is used as an output for the coarse (outer) grid and the fluxes as an input for the finer (inner) grid. These models are applicable to the case of wave propagating from the coarse grid domain to the finer grid domain. However, in the opposite direction, shorter waves leaving the inner grid domain, a considerable percentage of the energy is reflected back from the existing boundary keeping them trapped in the inner domain. Such trapped tsunami energy builds up as numerical errors and may cause numerical instabilities.

Fine resolution of digital topographic/bathymetric data-sets are quite available in coastal region of Japan; available in 2m to 50m resolution under a Cartesian coordinate system. These data-sets are effectively applied to numerical simulation of near-field tsunami and runup calculations. On the other hand, numerical simulation of trans-oceanic propagation of far-field tsunami is conducted based on a spherical coordinate system. Nesting two domains with different resolutions and/or coordinate systems brings some inconveniences when modelling tsunami. Usually numerical errors are manifested in the nested (inner) grid boundaries or inner domain as reflected or trapped waves. There is an extra effort for modeller to do conversion of mesh size to match common points of the inner and outer grids domain system. Therefore, this study aims to develop a tsunami numerical model which is capable to include several grid systems and facilitate the process of assembling domains of different resolutions. The assembly of structured domains (inner and outer) is achieved by constructing an intermediate unstructured grid or connector-domain between them. This connector-domain admits a smooth transition of physical process between the inner and outer domains. A numerical simulation consisting of a tsunami Gaussian-hump shape is used for validation of the connection by determining the energy transferred or retained in the inner domain. In addition a practical application, the 2010 Chilean Tsunami, is provided as a case study to confirm the validity of the proposed model.

2. INTEGRATION OF DIFFERENT GRID SYSTEMS

The integration of different grid systems is presented here. The connector-domain is located between structured grid domains which have different grid sizes as shown in Fig. 2.1. The outer and the inner domain are built as structured grid, the connector-domain is built as a combination with triangular unstructured grid and structured grid. Thus, calculations in the outer and inner domain are conducted by the Finite Difference Method (FDM), and the Finite Volume Method (FVM) is applied in the connector-domain. Numerical model of Goto et al. (1997) for the FDM and that of Kawaike et al.(2002) for the FVM are adopted, both models are based on the leap-frog scheme, i.e., second-order accurate in time.

To accommodate data exchange between the two models, line discharge fluxes are defined on the each domain’s boundary in the red bold line in Fig. 2.1. In the case of the calculation for the linearized shallow water equations, for instance, a pressure term which is required for the determination of line discharge fluxes can be calculated taking surface elevations of FDM grid and that of FVM grid. This is an advantage of this technique that variables in each domain can be delivered directly unlike conventional nesting technique which interpolates variables from outer to inner grids.

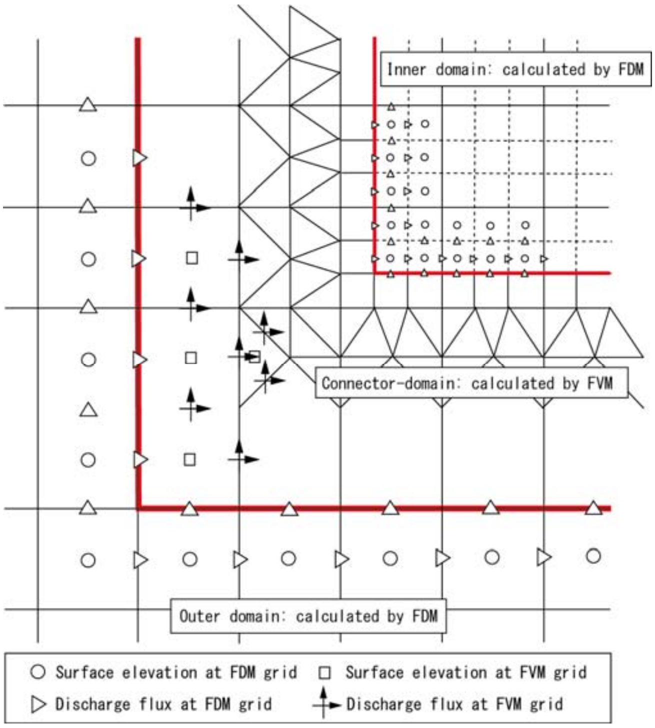

Figure 2.1. Schematic of integration of different grid systems. The red lines indicate boundaries of each domain.

3. TEST OF MODEL

3.1. Numerical setup

To test the accuracy of the present numerical scheme, a numerical simulation is conducted for the propagation form the initial profile of the Gaussian hump. The initial free surface condition is defined as:

$$\eta(x,y) = H\exp\left[-\frac{1}{a^2}\left\{(x-x_0)^2 + (y-y_0)^2\right\}\right], \tag{3.1}$$

where η is the surface elevation, H is the initial height of the hump at its center (x_0, y_0) and a is the characteristic horizontal length-scale of the Gaussian hump. This test case uses H=2.0 m, a=2,500 m, (x_0, y_0) = (0.0, 0.0), and initial velocity field is set to zero. The Gaussian hump initial condition is very useful for this test as the resulting water surface disturbance radiates in all directions; there is no dominant propagation direction. The linearized shallow water equations are solved to obtain numerical solutions.

Figure 3.1 illustrates the physical layout of the basin and numerical setup. The basin is considered a 540 km wide, 540 km length, and 4 km constant depth. The sponge layers with several dummy grids are applied at the edge of numerical domain as the open boundary condition. We conducted four cases of numerical conditions that are shown below.

Case 1: The inner domain with grid length of 0.6 km is located in the centre of basin. The outer domain has 1.8 km grid length as shown in Fig. 3.1. The conventional method that uses the 2-way nesting scheme by Goto et al.(1997) is adopted.

Case 2: The connector -domain is considered as 3.6 km wide (equal to the 2 grids of outer domain). 2,960 elements are located as shown in Fig. 3.2, in left panel. It is solved by the coupling model with the FDM and the FVM.

Case 3: The connector-domain is considered as 72 km wide (equal to the 20 grids of outer domain). 36,672 elements are located as shown in Fig. 3.2, in right panel. This condition is equivalent to one wavelength in this experiment.

Case 4: Structured grids of 0.6 km length are set in entire domain. The FDM is adopted.

In all cases, the time step is set to 0.5 sec.

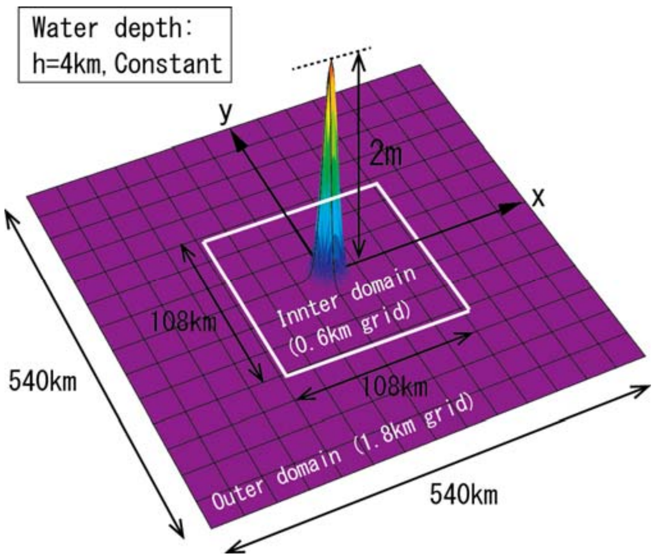

Figure 3.1. Physical concepts of Gaussian hump simulations and numerical setup for Case 1.

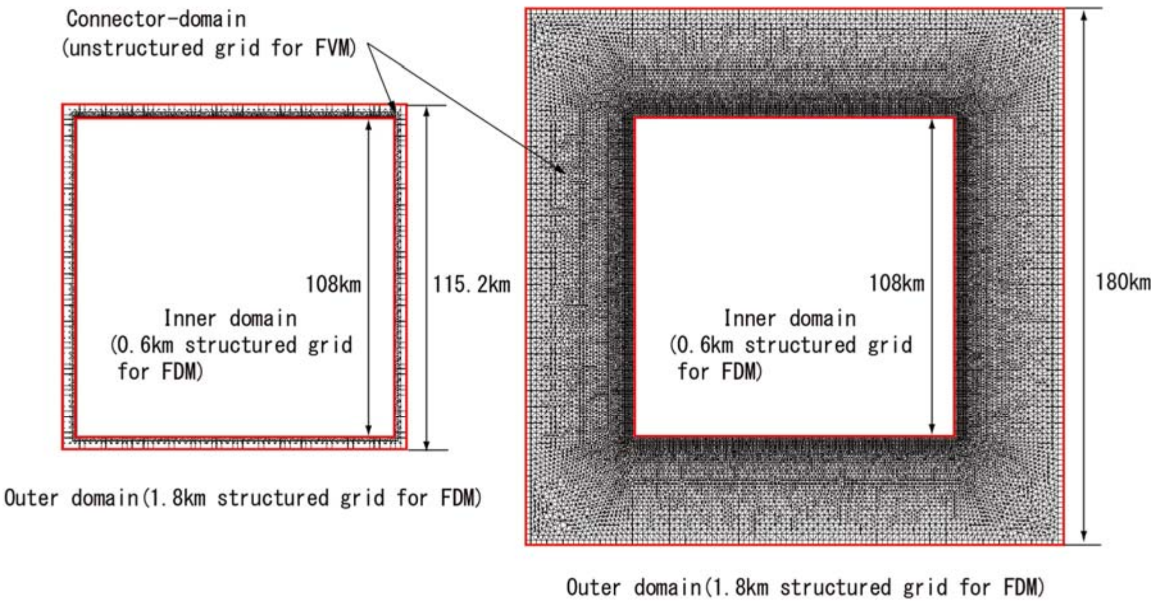

Figure 3.2. Unstructured grids for connector-domain. Case 2, left panel. Case 3, right panel. Grid construction for Case 2 corresponds to Fig. 2.1. The red lines indicate boundaries of each domain.

3.2. Simulation results

Figure 3.3 shows the numerical results of water surface distribution in the inner domain at t=350 s for Case 1, 2 and 3. In this simulation, the exact physical solution implies that any waves must not exist in the inner domain after the waves pass through the outer domain. In Case 1, conventional 2-way nesting scheme, small reflected wave is generated from the boundary between the inner and the outer domain, and they are propagating toward the center direction of the inner domain. The magnitude of reflected wave is around 10% of that of the progressive wave. The result of Case 2 is the coupling model with the FDM and the FVM considered the connector-domain. However, the reflection waves are also generated the same as Case 1 because the size of unstructured grids suddenly changed in short-distance for one-structure grid of the outer domain. On the other hand, in the result of Case 3, this is the case that the unstructured grid sizes gradually changes in the connector-domain, no reflected waves is observed on the boundary; they are perfectly transmitted to the outer domain. The Case 3 provides appropriate results from this experiment.

The comparison of computing time in each case is shown as Table 3.1. The computing time is measured by using Intel Xeon processor (3.0 GHz) for the simulation and “Time Ratio” is defined as (CPU time in each case) / (CPU time in Case 3). The present model of Case 3 requires CPU time about two-times more than that of the conventional 2-way nesting scheme of Case 1. However, around half of Case 4 which grid size in the entire domain equal to that of the inner domain (0.6 km). This is one of the advantages arising from integrating the two models.

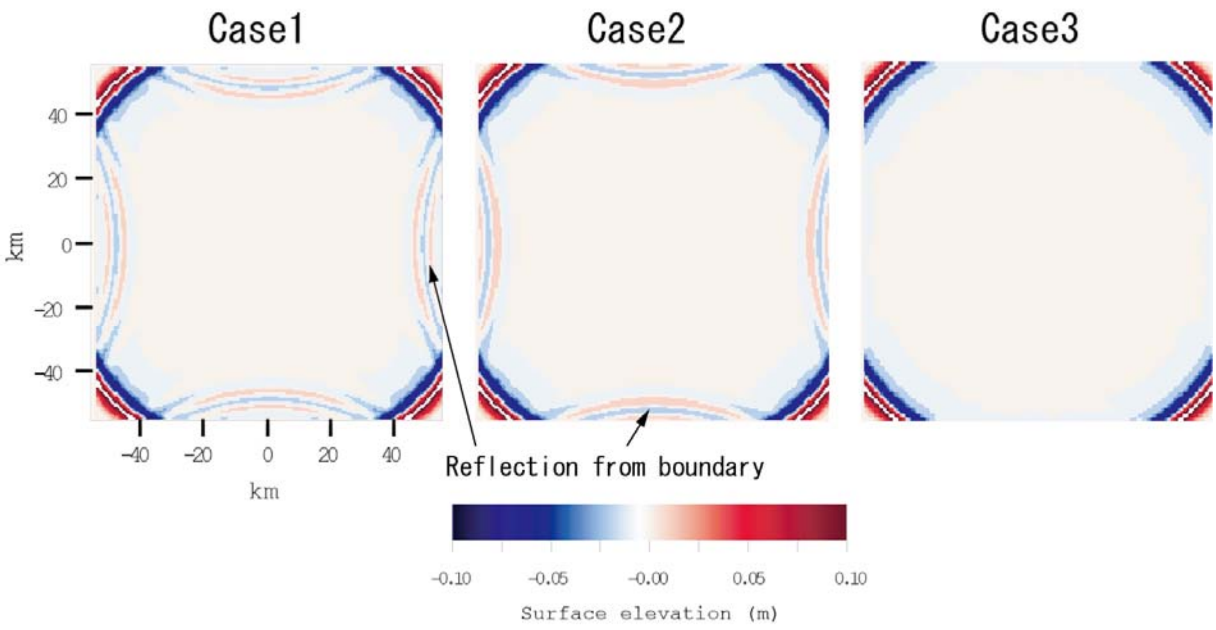

Figure 3.3. Snapshots of propagation of Gaussian hump in inner domain at t=350s for Case 1 to 3.

Table 3.1. Comparison of computing time in each case. The total time loop counts of simulation are 1,500.

Case	Model	Grid number		Time(s)	Time Ratio
		FDM(Outer + Inner)	FVM(Connector)		
1	FDM	300×300+180×180	0	21.0	0.37
2	FDM&FVM	298×298+180×180	2960	23.5	0.41
3	FDM&FVM	280×280+180×180	36672	56.6	1.00
4	FDM	1200×1200	0	106	1.85

4. NUMERICAL SIMULATION OF 2010 CHILEAN TSUNAMI

As a practical test, the present model is applied to the tsunami event of 2010 Chilean earthquake. The computed results were compared to observed surface elevations and velocities to verify the model.

4.1. Numerical setup

The bathymetric and topographic data and grid system has been organized to simulate 2010 Chilean tsunami using the integration of different grid system. Figure 4.1 shows the seismic deformation induced by the 2010 Chilean earthquake within the entire computational domain, covering from (120°E, 60°S) to (70°W, 60°N). Open ocean bathymetry and topography is taken from the GEBCO database in 5 arc minutes interval. Figure 4.2 depicts coverage of computational domains vicinity of Japan. The connectr-domain corresponds to the white line in Fig. 4.1, left panel. This domain is composed of unstructured grids and the still water depth at each grid is interpolated from several data-sets of structured grid; the free distributed database in coastal region of Japan whose spacing of 10, 50, 150 and 450 m in Cartesian coordinate system, and the GEBCO database of 0.5 arc-min grid in spherical coordinate system. The detailed bathymetry and topography of inner domain in Kesen-numa bay is shown as Fig. 4.2 right panel. It is composed of structured grids the size of 1/3 arc-second (10 m, approximately).

The generation of an initial surface condition is based on the provide fault model of Yanamaka (2010); the parameters are listed on Table 4.1. The nonlinear shallow water equations in spherical coordinate system are applied for the governing equation. The runtime of simulation is set to 30 hour of physical time. The time step is set to 10 s until 24 hour from the initial time, after that it is changed to 0.2 s.

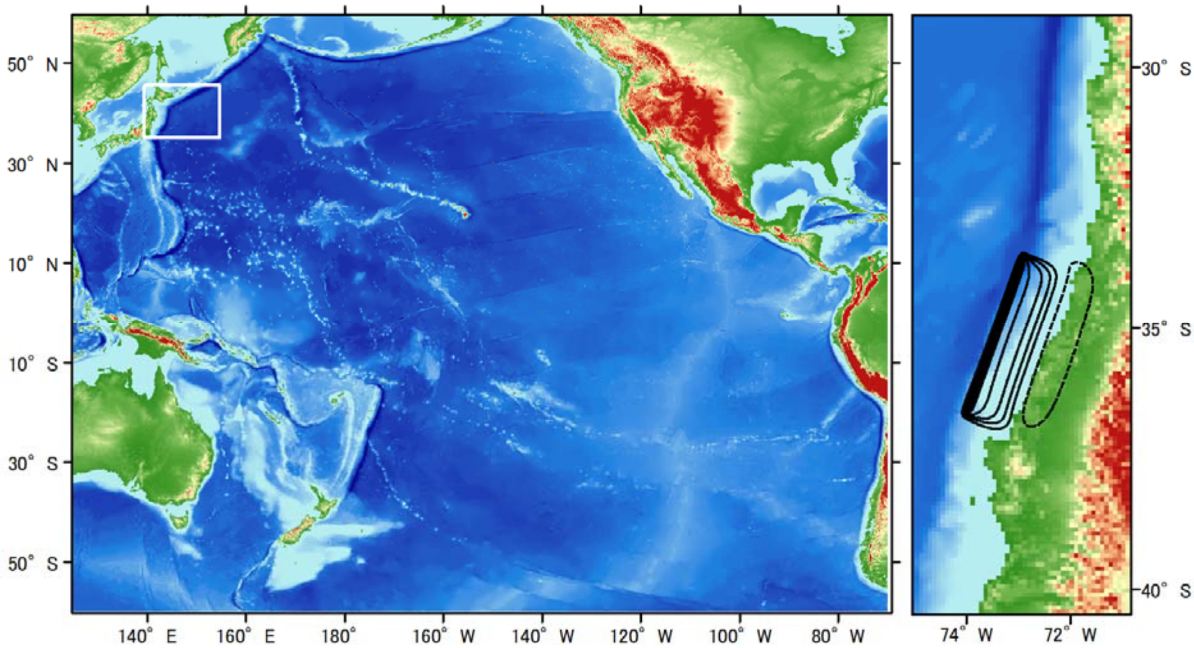

Figure 4.1. Bathymetry and topography in the model region for the 2010 Chilean Tsunami. 5-arc minutes computational domain (left) and close-up view of seismic deformation. The contour interval is 0.5m (right). The solid lines indicate for uplift and the dashed lines for subsidence.

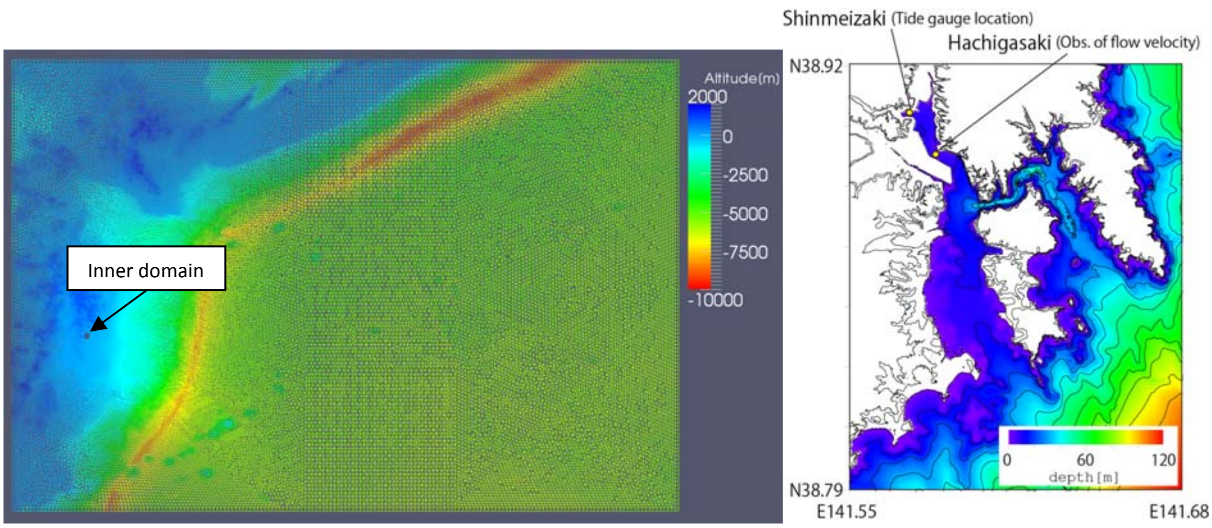

Figure 4.2. Coverage of computational domains vicinity of Japan. Connector-domain composed of unstructured grids which corresponds to the white square in Fig.4.1 (left) and inner domain of Kesen-numa bay, composed of structured grids (right).

Table 4.1. Fault parameters for 2010 Chilean earthquake.

Longitude, Latitude, Focal depth	73.959°W, 36.652°S, 4.63 km
Length, Width	360 km, 100 km
Strike, Dip, Slip	18°, 20°, 105°
Dislocation	6.94 m
M_w	8.76

4.1. Results and discussion

In the 2010 Chilean tsunami event, observation equipment, i.e., GPS buoy system of Japan (deployed by Ministry of Land, Infrastructure, Transport and Tourism) and DART buoys by NOAA recorded the physical tsunami waveform. As one of result, the comparison of the observed and computed surface elevations at GPS buoy station is shown in Figure 4.3. The GPS buoy at Off South Iwate is located at 142.097°E, 39.259°N, 204 m depth. Although the computed result of tsunami heights is fairly consistent with observed, note that the computed result shown in this section is shifted the time series to backward by 30 minutes. Kato et al. (2011) pointed out that the observed tsunami arrived about 30 minutes later than the arrival time predicted by the numerical simulation. The difference in arrival times of about 30 minutes may have to be investigated by considering various factors such as the sea bottom topography features on the path of the tsunami propagation, the spatial resolution of gridding, modeling errors, the effect of dispersion, etc.

To confirm the verification of computed results in the inner domain, observed surface elevations at tide gauge and flow velocities are compared to the computed results. Figure 4.4 shows the comparison of the observed and computed surface elevations at tide gauge of Shinmeizaki in Kesen-numa bay (for detailed location, see Fig. 4.2 right panel). The computed tsunami heights are significantly agreement with the observed. Flow velocities are obtained by using PTV (Particle Tracking Velocimetry) image analysis. Trajectories of debris displacement accompanied by tsunami flows were measured from the several video images taken in this event at Hachigasaki as shown Fig. 4.5 left panel, then velocities could be calculated from derivation of the displacement. Thus, the measured velocities and its directions at each time are summarized in Fig. 4.5 right panel. Figure 4.6 shows the comparison of the observed and the computed flow velocity. As the observed velocities have a fluctuation, the computed results are overwriting at nine points around the observed area. The velocity obtained by the simulation is around half of the observed; however, the behaviour of tsunami was reproduced successfully as shown Fig. 4.7. Considering the numerical error on velocity, flow velocity might be larger than this result.

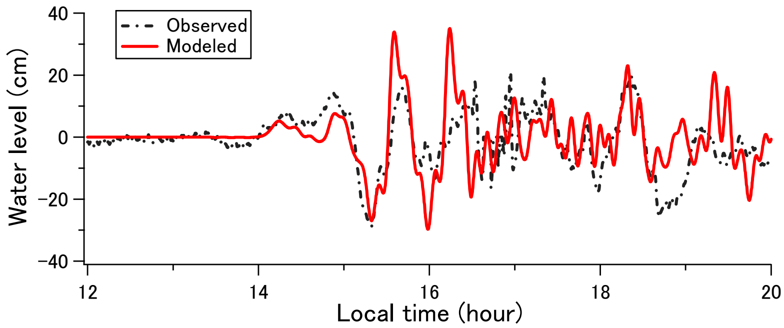

Figure 4.3. Time series of surface elevations at GPS buoy station (Off South Iwate). The computed result is manually shifted time series to backward by 30 minutes.

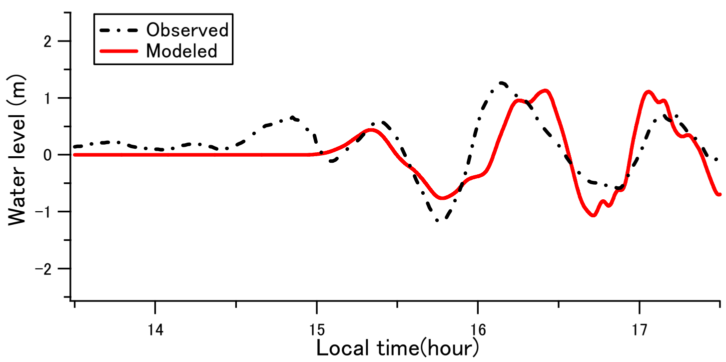

Figure 4.4. Time series of surface elevations at tide gauge of Shinmeizaki in Kesen-numa bay.

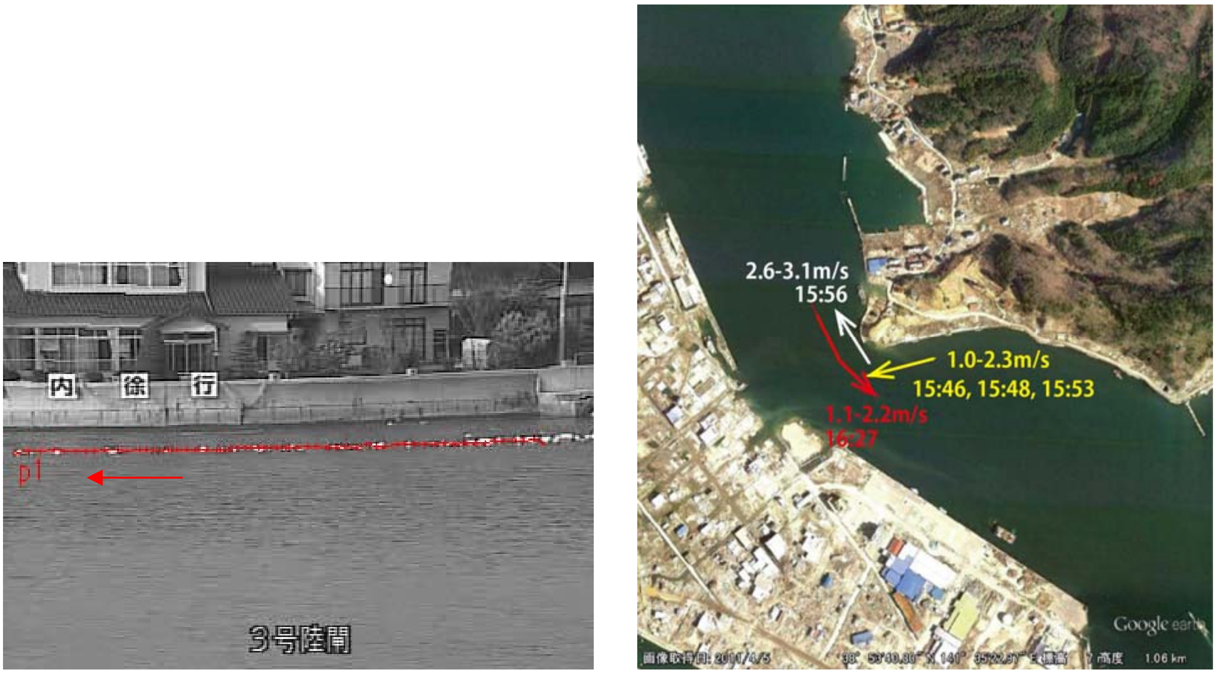

Figure 4.5. Trajectory of debris by PTV image analysis (left) and summary of observed tsunami flow in each time on JST (right).

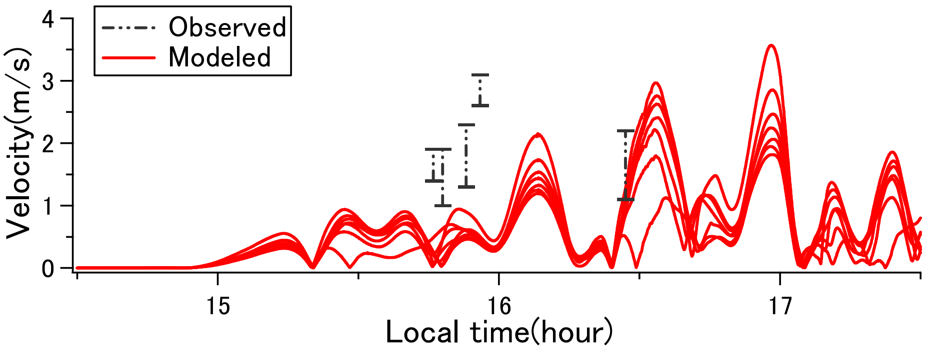

Figure 4.6. Time series of magnitude of flow velocity at Hachigasaki in Kesen-numa bay.

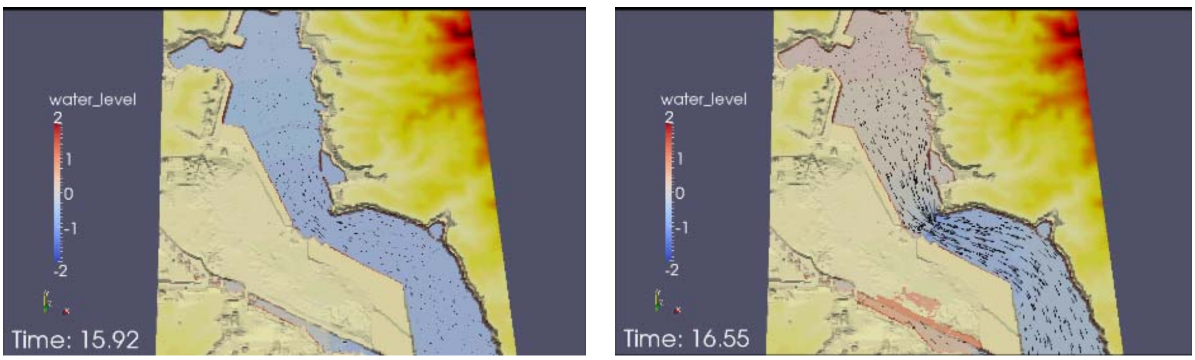

At 15:55 JST.

At 16:33 JST.

Figure 4.7. Snapshot of computed surface elevation and velocity vector around Hachigasaki in Kesen-numa bay.

5. CONCLUSIONS

This study has developed a numerical model that integrated several difference grid systems for tsunami simulations. The important framework of this model is as follows: The connector-domain is built as the unstructured grids between outer and inner domains which are built as structured grids. Thus, calculations in outer and inner domain are conducted by the Finite Difference Method, and the Finite Volume Method is applied in the connector-domain. To test the accuracy of the present numerical scheme, a numerical simulation is conducted by using a Gaussian wave which propagates from the inner to the outer domain. The result of the proposed methodology is compared with a conventional model that has numerical error at the boundary between the inner and the outer domain, the present model provides appropriate results from this experiment. As a practical test, the present model is applied to the tsunami event of 2010 Chilean earthquake. The computed results were compared to observed surface elevations and velocities to investigate model validity. The water elevation reproduced by the simulation agreed with the tide-gage data measured at the bottom of Kesen-numa bay, considering a time difference of 30 minutes. The velocity obtained by the simulation was around half of the observed value obtained by analysing a video; however, the behaviour of tsunami was reproduced successfully.

AKCNOWLEDGEMENT
The observed data of GPS buoys was provided by the Ministry of Land, Infrastructure and Tourism (MLIT).

REFERENCES

Kowalik, Z. and Murty, TS. (1993). Numerical modeling of Ocean Dynamics. World Scientific, Singapore.

Goto, C., Ogawa, Y., Shuto, N. and Imamura, F. (1997). IUGG/IOC time project: numerical method of tsunami simulation with the leap-frog scheme. *Manuals and Guides*, **no. 35**, Intergovernmental Oceanographic Commission of UNESCO, Paris.

Yamazaki, Y., Cheung, KF. and Kowalik, Z. (2010). Depth-integrated, non-hydrostatic model with grid nesting for tsunami generation, propagation, and run-up. *International Journal for Numerical Methods in Fluids* **67:12**,2081-2107.

Son, S., Lynett, P. and Kim, D.-H. (2011). Nested and multi-physics modeling of tsunami evolution from generation to inundation. *Ocean modeling*, **38**: 96-113.

Kawaike, K., Inoue, K., Hayashi, H. and Toda, K. (2002). Development of inundation flow model in urban area. *J. of Hydraulic, coastal and Environmental Eng., JSCE*, **698:II-58**,1-10 (in Japanese).

Yamanaka, Y. (2010). http://www.seis.nagoya-u.ac.jp/sanchu/Seismo_Note/2010/NGY25.html

Kato, T., Terada, Y., Nishimura, H., Nagai, T. and Koshimura, S. (2011). Tsunami records due to the 2010 Chile earthquake observed by GPS buoys established along the Pacific coast of Japan. *Earth Planets Space*, **63**, e5-e8.